Polymer Testing 104 (2021) 107411

Contents lists available at ScienceDirect

Polymer Testing

journal homepage: www.elsevier.com/locate/polytest

The influence of particle chain-magnetic field spatial location, frequency, dynamic strain amplitude and the prestrain on the mechanical performance of anisotropic magneto-rheological elastomer

Bochao Wang [a,1], Yan Li [a,1], Yingduan Gao [a], Jingyi Zhang [a], Zhenbang Xu [b], Jun Li [c], Ji Li [c], Leif Kari [d,**], Yu Wang [a,***], Xinglong Gong [a,*]

[a] CAS Key Laboratory of Mechanical Behavior and Design of Materials, Department of Modern Mechanics, University of Science and Technology of China, 230027, Hefei, China
[b] CAS Key Laboratory of On-orbit Manufacturing and Integration for Space, Optics System, Changchun Institute of Optics, Fine Mechanics and Physics, Chinese Academy of Sciences, 130033, Changchun, China
[c] Anhui Weiwei Rubber Parts Group Co. Ltd., 231460, Tongcheng, China
[d] KTH Royal Institute of Technology, Department of Engineering Mechanics, The Marcus Wallenberg Laboratory for Sound and Vibration Research (MWL), 10044, Stockholm, Sweden

ARTICLE INFO

Keywords:
Anisotropic magnetorheological elastomer
Particle-chain-magnetic field spatial location
Magnetorheological effect
Strain dependent viscoelasticity
Prestrain

ABSTRACT

Although there are literatures to characterize the properties of anisotropic magneto-rheological elastomer (MRE), more attention is paid when the particle chain is parallel to the applied magnetic field. However, in prospective of modeling and application design, mechanical characterization of anisotropic MRE under other particle chain-magnetic field spatial locations is needed. Herein, mechanical properties of anisotropic MRE with four kinds of particle chain-magnetic field spatial locations under varies frequencies, strain amplitudes and prestrains are tested. It shows that even the particle chain is perpendicular to the magnetic field, there exists an obvious MR effect. Besides the attraction of adjacent magnetized particles, the Maxwell stress tensor also contribute to the MR effect. Furthermore, an obvious strain amplitude dependent viscoelastic behavior is exhibited for anisotropic MRE. Moreover, the MR effect and the loss factor decrease as the increase of prestrain. The investigation contributes to the designing, modeling and applications of anisotropic MRE.

1. Introduction

Smart materials which can perceive and respond to external stimuli, such as temperature, PH level, electric and magnetic field have received extensive attention during the past few decades [1]. As an important branch of magneto-sensitive smart material, magnetorheological elastomer (MRE) shows a great potential for many engineering applications [2]. For most applications, MREs are prepared by imbedding ferromagnetic particles of micro/nano-scale into a polymer matrix. Depending on the absence or presence of the magnetic field during the vulcanization process and the subsequent orientation of the particles, MREs can be divided into either isotropic or anisotropic.

In the early stage of fabrication, mainly soft magnetic materials such as iron particles or carbonyl iron powder are imbedded in the polymer matrix of MREs. Due to the internal interaction between soft magnetic particles and polymer matrix, the stiffness and damping properties of MREs can be varied when an external magnetic field is applied [3]. Owing to the magnetorheological (MR) effect of MRE, that is, the increase in modulus with increasing magnetic field, many investigations for the possible application of MRE in the area of vibration and noise attenuation have been conducted. MRE-based absorbers with a shifting frequency property were designed and the vibration reduction effect was studied [4–7]. Adaptive isolators based on MREs by changing stiffness were designed and explored as well [8–17]. Recently, it has been found that besides the MR effect, MRE also displays magneto-induced deformation ability by adding hard magnetic fillers like Fe3O4 [18] and

* Corresponding author.
** Corresponding author.
*** Corresponding author.
E-mail addresses: leifkari@kth.se (L. Kari), wyu@ustc.edu.cn (Y. Wang), gongxl@ustc.edu.cn (X. Gong).
[1] These authors contributed to the work equally and should be regarded as co-first authors.

https://doi.org/10.1016/j.polymertesting.2021.107411
Received 25 August 2021; Received in revised form 11 October 2021; Accepted 4 November 2021
Available online 6 November 2021

NdFeB [19] into the polymer matrix. Therefore, in addition to the traditional applications of MRE in vibration control, there were investigations regarding the applications of MRE in morphing tools [20], soft robotics [21] smart pump [22] and surface roughness active control [23,24]. Besides, by mixing electrical conductive materials, like AgNW [25,26] and liquid metal [27] to increase the conductivity of MRE, an electrical resistance change under different strain ampliutde is exhibited for MRE, therefore, it is promising to fabricate a soft sensor that integrates strain and magnetic sensing functions by MRE.

In order to customize MRE-based devices/structures for engineering applications, it is necessary to characterize the magneto-mechanical performance of MRE experimentally and theoretically. Regarding the theoretical modelling, micromechanically based theory, rheology theory and continuum mechanics have been utilized to predict the magneto-mechanical behavior of MRE. By utilizing the micromechanically based theory, a one-dimensional quasi-static model of MRE which accounts for magnetic nonlinearities and saturation by extending a simple magnetic dipole interaction model was developed [28]. Chen et al. [29] and Zhu et al. [30] further extended the dipole based model by introducing the viscoelastic behavior of MREs and the multi-chain interactions. Garcia-Gonzalez et al. [31] extended the dipole-dipole interaction model to take into account the effect of attraction force for hard magnetic particle based-MRE on the initial stretch of polymer matrix network. Han et al. [32] proposed a wavy particle chain dipolar interaction model for MRE to predict the field-stiffening effect of MRE in tension and compression. By combining continuum mechanics and microscopic approach, Ivaneyko et al. [33] developed a theoretical model which can analysis the magneto-mechanical performance of MRE with different shapes and particle distributions and Garcia-Gonzalez et al. [34] proposed a theoretical model for MRE which can taking viscous dependences and magneto-mechanical coupling into account. By means of finite-strain homogenization [35–37], the macroscopically nonlinear magneto elasticity of MREs can be depicted by solving the average response of the microscopic representative volume element of MREs.

In addition to the micromechanically based method, rheology theory have been utilized to predict the dynamic behavior of MRE under different magnetic fields, frequencies, strains and temperatures [38–42]. However, due to the technical difficulties associated with geometrical nonlinearity, the rheology theory based models were limited to the small strain regime. By combing electromagnetic theory and continuum mechanics, an extend Helmholtz free energy function with deformation gradient and magnetic flux density as independent variables was proposed and the magneto-elastic behavior of isotropic MRE was modeled [43,44]. Saxena et al. [45], Danas et al. [46], Bustamante [47], Shariff et al. [48] and Wang et al. [49,50] further extended the model to predict the viscoelasticity, anisotropy, strain amplitude and temperature dependent nonlinear behavior of MREs. Haldar et al. [51] embedded a constitutive model of MRE with a rate dependence and magneto-mechanical coupling into finite element simulations. By stipulating that the magnetic flux density is linearly dependent on the applied magnetic field strength, Zhao et al. [52] developed a model which depicts the relation between the magnetic field and the magnetic field induced deformation of hard-magnetic-filler based MREs. Danas et al. [53,54] utilized an energy-based continuum mechanical method to analyze the bifurcation of MRE based film which is bonded to a non-magnetic substrate. However, it should be noted that currently only magneto-hyper-elastic behavior is modeled for anisotropic MRE. However, as a special kind of filler rubber, besides hyper-elastic behavior, there is a pronounced strain amplitude dependent viscoelastic behavior with a strong directionality of anisotropic MRE. To stimulate the constitutive modeling of the dynamic behavior of anisotropic MRE, more characterization and measurement data of the dynamic behavior of anisotropic MRE is needed.

The dynamic shear modulus of isotropic MRE under different magnetic fields, frequencies and strain amplitudes was experimentally determined [55–59]. Bodelot et al. [60,61] investigated the particle-polymer interfacial adhesion and the coupled magneto-mechanical performance of MRE. Although the dynamic performance of anisotropic MRE under different strain rates, magnetic fields, strain amplitudes, prestrains [62–64] has been determined, it is only applicable to the case where the particle chains are parallel to the external magnetic field [65–69]. In order to reveal the in plane angle between the particle chain orientation and the applied magnetic field on the magneto-mechanical behavior of MRE, the dynamic shear modulus and magneto-deformation of anisotropic MRE under different in-plane particle chain-magnetic field angles and frequencies were measured [70,71]. Abramchuk et al. [72,73] determined the static magneto-mechanical behavior of isotropic and anisotropic MRE under compression and proposed a phenomenological model to reflect the effect of applied magnetic field on the elastic modulus of MRE. Tian et al. [74] fabricated silicone based anisotropic MRE where the iron particle chain is 45° to the flat MRE direction and characterized its asymmetry mechanical performance along different pure shear direction experimentally.

In practical applications, it is not common that the particle chain structure of anisotropic MRE is not parallel or even not coplanar with the magnetic field. However, compared with isotropic MRE, the coupling among the particle chain-like structure, the deformation field and the magnetic field of anisotropic MRE are more significant and complex. Therefore, for the completeness of the mechanical characterization of anisotropic MRE, it is necessary to test the mechanical behavior of anisotropic MRE under the above mentioned unusual particle chain-magnetic field spatial locations. Refer to the theory by Bustamante [47] and after derivation (please check the appendix for more details), it can be found that under simple shear test, mechanical characterization of anisotropic MRE under the following four kinds of particle chain-magnetic-deformation spatial location test settings as in Fig. 1 are needed for the completeness of the characterization of the magneto-elastic performance and the identification of the material parameters. Although Varge et al. [75] measured the mechanical performance of anisotropic MRE under the above mentioned test settings, only elastic behavior was considered. The strain amplitude dependent viscoelastic behavior and the effect of the prestrain on the mechanical performance of anisotropic MRE are not taken into account. However, an accurate characterization for the effect of the strain amplitude dependent viscoelasticity and the prestrain on the mechanical behavior of anisotropic MRE is the prerequisite to achieve a desired vibration control effect for the application of MRE in vibration control area.

To fully clarify the factors which influence the magneto-mechanical behavior of anisotropic MRE and to guide the application and constitutive modeling, the characterization of the magneto-mechanical properties of anisotropic MRE under varies particle chain-magnetic field spatial locations with different magnetic field strengths, frequencies, strain amplitude and prestrains are conducted in this manuscript. The structure of this manuscript is as follows. In Section 2, the fabrication procedure of anisotropic MRE, the test machine setup and the characterization method are introduced. The quasi-static and dynamic mechanical test results of anisotropic MRE under different particle chain-magnetic field spatial distributions, magnetic field strengths, frequencies and strain amplitudes are conducted and their effects on the mechanical behavior of MRE are analyzed in Section 3. Considering that MREs may encounter prestrain in practical engineering applications due to static loading, the effect of prestrain on the dynamic behavior of MREs is investigated in Section 4. Finally, a brief conclusion and an outlook are given in Section 5. The work in this manuscript helps deepening the understanding on how the microscopic distribution of particles, the magnetic field and the deformation field affect the magneto-mechanical behavior of MREs. Furthermore, the results obtained from the characterization in this work can be used to enhance the constitutive modeling and enlarge the potential application area of MREs.

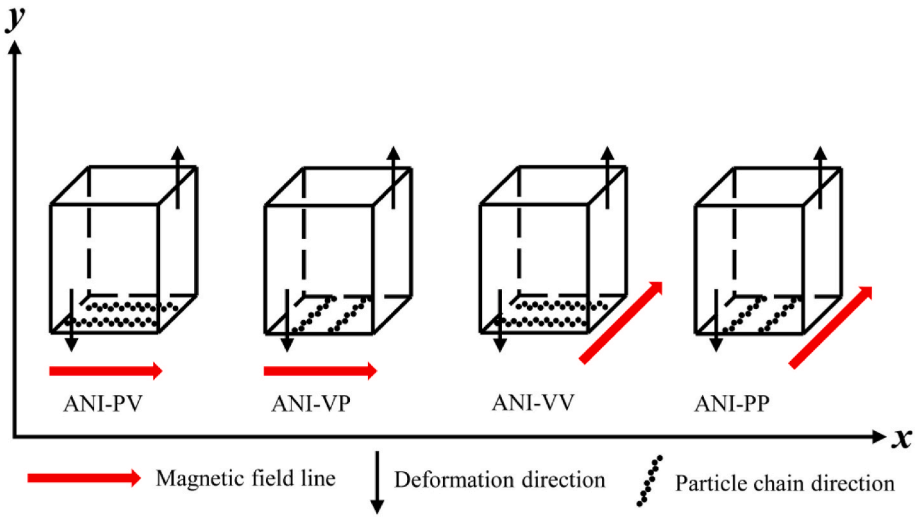

Fig. 1. Four kinds of test settings for anisotropic MRE under simple shear. ANI represents anisotropic. The first letter after the dash symbol represents the spatial distribution between the particle chain direction and the magnetic field. The second letter represents the spatial distribution between the particle chain direction and the deformation plane. Letter "P" stands for parallel and letter "V" for vertical.

2. Material preparation and test method

2.1. Material fabrication and measurement setup

The raw materials used to fabricate anisotropic MRE include carbonyl iron particles (CIPs, type CN, BASF, Germany diameter 7 μm on average), polydimethylsiloxane (PDMS) and curing agent. The PDMS and curing agent belong to Sylgard™ 184 silicon elastomer kit, purchased from Dow Corning, United States. For the anisotropic MRE in this manuscript, the mass ratio for carbonyl iron particle, PDMS and curing agent are 45: 30:1 and the actual measured of these three component are 105.68 g, 70.46 g and 2.35 g, respectively. Two kinds of anisotropic MRE samples were prepared for the subsequent characterization. After mixture the PDMS, carbonyl iron particle and curing agent for about 5 min, the mixture was placed in a vacuum chamber with a pressure of 0.06 MPa for 10 min to remove the air bubbles. For type A MRE, the particle chain direction is along the y-axis of the mold, and for type B MRE, the particle chain direction is along the z-axis of the mold, as shown in Fig. 2. To fabricate anisotropic MRE samples, after sealing, the mold (6061 typed aluminum alloy with a minimum surface roughness of Ra 1.6) was placed on a heater, also shown in Fig. 2, under a magnetic of 0.7 T and a temperature of 100 $^{\circ}C$ for half an hour. To guarantee that the magnetic flux within type A and type B has the same value, a Tesla meter is inserted into the area close to the mold and the current applied two the two electromagnets is adjusted to make sure that the magnetic field strength measured by the Tesla meter for Type A and B MRE are totally the same.

A dynamic mechanical analyzer (DMA) typed Electro-Force 3200 from TA Instruments Inc. was utilized to characterize the static and dynamic mechanical performance of MRE samples. The photograph and the schematic configuration of the DMA are shown in Fig. 3. In order to reflect the effect of the magnetic field strength on the mechanical performance of MREs, two electromagnets placed in parallel were used to generate the magnetic field. Four magnetic field strengths, 0, 0.17, 0.34 and 0.51 T, were applied to the test samples during the measurement. Although there exists a stronger MR effect after 0.51 T, the upper limit of

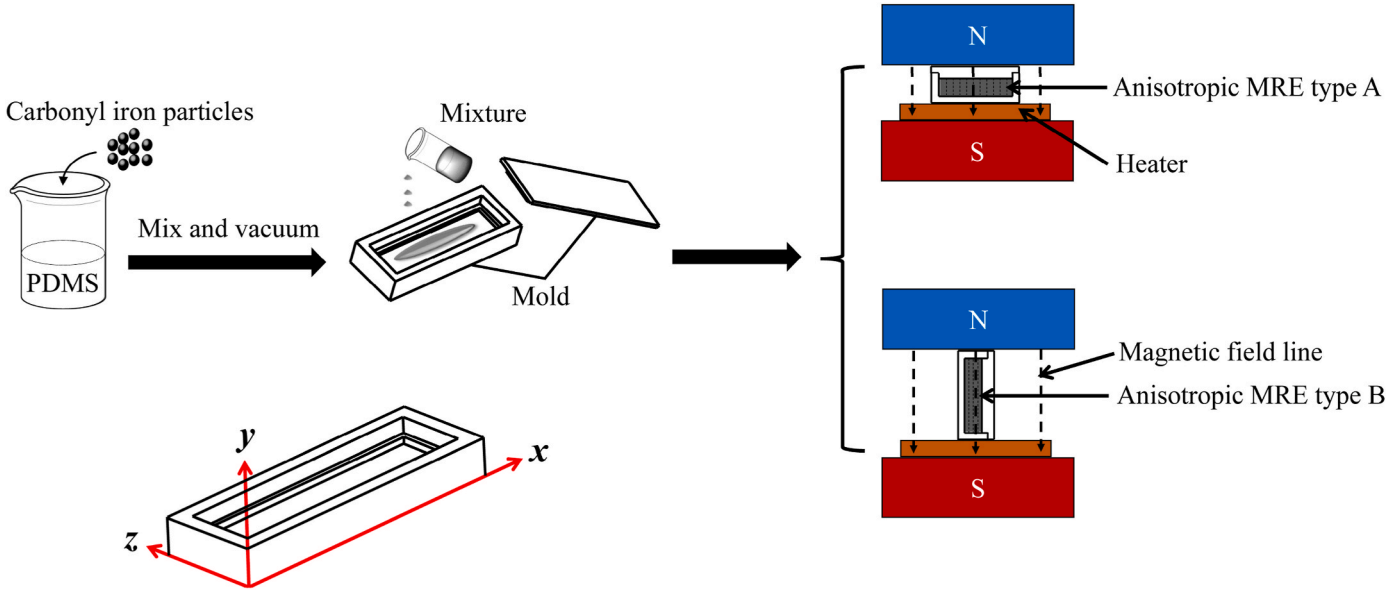

Fig. 2. Schematic configuration of the fabrication process of anisotropic MREs.

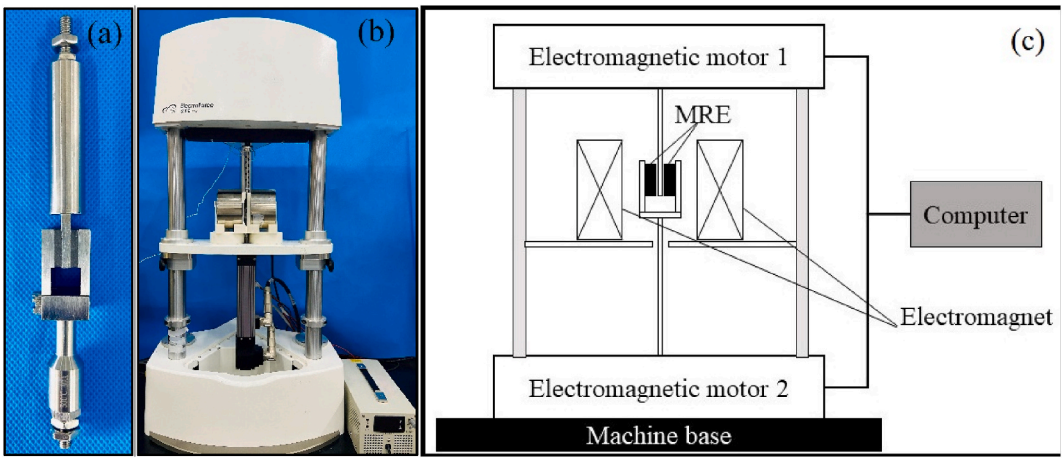

Fig. 3. Photograph of the shear fixture (a), photograph (b) and schematic configuration (c) of the dynamic mechanical analyzer with magnetic field excitation function.

the magnetic field strength is nevertheless set to be 0.51 T since the generation of a stronger magnetic field strength is also accomplished by a sharp rise of temperature of the electromagnet which may affect the test result. During the test, although the magnetic permeability of the MRE is different from that of air, the magnetic flux density measured in the air is the same as that within the MRE according to the continuous condition of the normal component of the magnetic flux density.

Two MRE samples, where the width (x-axis), height (y-axis) and length (z-axis) are 2 mm, 12.9 mm and 15.6 mm, are glued to the shear fixture of the DMA machine using the Ergo 5400 general purpose instant adhesive made in Switzerland. The simple shear deformation of the test samples as shown in Fig. 1 is

$$\mathbf{F} = \begin{bmatrix} 1 & 0 & 0 \\ \gamma & 1 & 0 \\ 0 & 0 & 1 \end{bmatrix}, \tag{1}$$

where $\mathbf{F}$ is the deformation gradient which connects the reference configuration (undeformed state) and the current configuration (deformed state) of the sample and γ is the deformation along the y-axis of the test sample.

To characterize the effect of the particle chain-magnetic field spatial location on the mechanical performance of MRE, four kinds of measurement setups, as shown in Fig. 1, are considered. In order to avoid the influence of the Mullins effect [76] on the test results, a repeated simple shear deformation with an amplitude of 0.4 mm, corresponding to 20% strain, at a frequency of 1 Hz was applied to the test samples prior to the main measurements. The repeated shear deformation was terminated when there is no further stress softening caused by the Mullins effect, that is, the strain-stress curves of two consecutive cycles overlap.

The scanning electron microscope images of the MRE samples are shown in Fig. 4. For images in Fig. 4, the magnification factor is 200. The left image in Fig. 4 is the cross section parallel to the direction of the applied magnetic field during curing of the anisotropic MRE. As shown in the image, the applied magnetic field during the curing process cannot guarantee that all the carbonyl iron particles are completely arranged in the same direction. The right image in Fig. 4 is the cross-section perpendicular to the direction of the applied magnetic field during curing of the anisotropic MRE. Due to the superposition and contribution of multiple chains, the distribution of carbonyl iron particles seems to be denser and more random compared with the left image in Fig. 4.

In order to analyze the effect of particle chain-magnetic field spatial location (parallel and perpendicular) on the magnetic performance of anisotropic MRE, the magnetization behavior of anisotropic MRE where the particle chain structure are either parallel (parallel alignment) or perpendicular (perpendicular alignment) to the applied magnetic field are measured by Hysteresis Measurement of Soft and Hard Magnetic Materials (HyMDC Metis, Leuven, Belgium) and the results are shown in Fig. 5.

Since PDMS and carbonyl iron particles are all soft magnetic

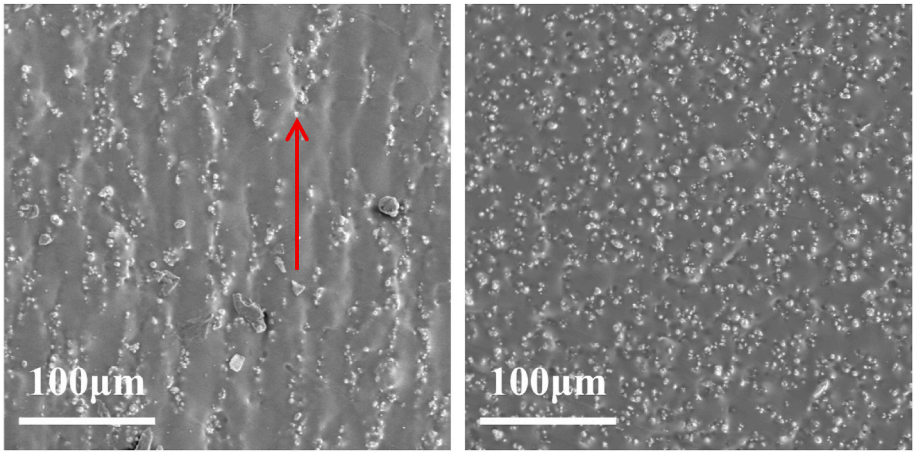

Fig. 4. Scanning electron microscope images of anisotropic MRE samples. The red arrow represents the direction of magnetic field during curing process. (For interpretation of the references to colour in this figure legend, the reader is referred to the Web version of this article.)

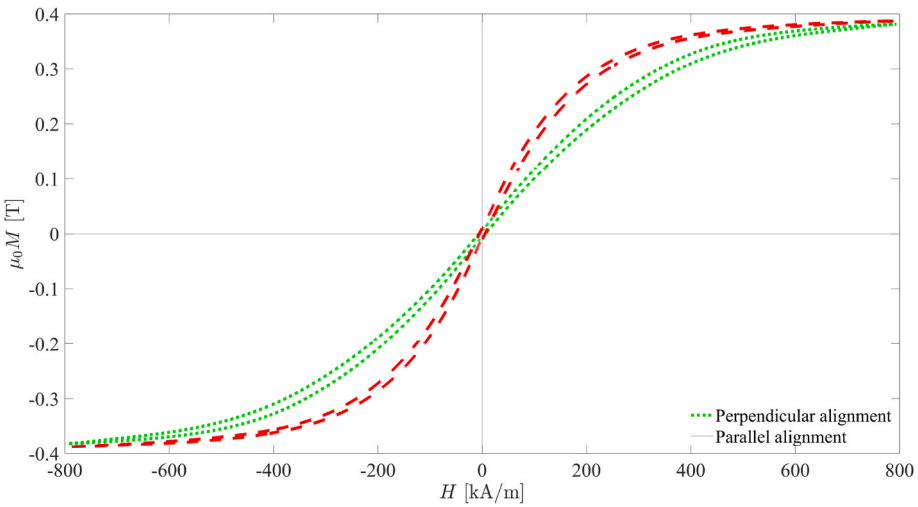

Fig. 5. Magnetization hysteresis loops for different particle chain-magnetic field spatial locations. Perpendicular alignment represents the particle chain structure is perpendicular to the applied magnetic field and parallel alignment represents that the particle chain structure is parallel to the applied magnetic field.

material, the areas enclosed by the two magnetic hysteresis loops are both very small. After conducting averaging and numerical computation, the magnetic susceptibility in the linear region of the magnetic hysteresis loops (from −100 kA/m to 100 kA/m) for the parallel alignment and the perpendicular alignment are 2.412 and 1.858, respectively. Furthermore, it can be found that the anisotropic MRE sample where the particle chain structure is parallel to the applied magnetic field is easier to be magnetized compared with the perpendicular one. Therefore, a larger MR effect is expected for the ANI-PV MRE sample. Since the saturation magnetization is a material constant, the saturation magnetization strength is the same (0.3873 T) for the two test cases.

2.2. Characterization method

Due to the effect of the geometrical nonlinearity, the traditional definitions of shear modulus and loss factor cannot be directly used to assess the effects of the magnetic field strength, frequency and the strain amplitude on the static and dynamic properties of MRE. However, in order to evaluate the effects of the magnetic field strength, frequency and the strain amplitude on the mechanical properties of MRE quantitatively, a Fourier transform-based method [77,78] is applied to extract the frequency response function $G^*(\omega)$ (complex shear modulus) of MRE, by the obtained stress τ and strain γ, reading

$$G^*(\omega) = G'(\omega) + \mathrm{j}G''(\omega) = \frac{\widetilde{\tau}}{\widetilde{\gamma}}, \tag{2}$$

where $G'(\omega)$ is the real part of $G^*(\omega)$ representing the equivalent storage modulus in frequency domain, j is the imaginary unit and $G''(\omega)$ is the equivalent loss modulus in frequency domain. The wavy superscript represents the Fourier transformation of the time domain signal to frequency domain.

After obtaining $G^*(\omega)$ and $G''(\omega)$, the equivalent shear modulus magnitude $|G^*(\omega)|$ and the equivalent loss factor $\eta(\omega)$ can be obtained by

$$|G^*(\omega)| = \sqrt{G'(\omega)^2 + G''(\omega)^2}, \tag{3}$$

and

$$\eta(\omega) = \frac{G''(\omega)}{G'(\omega)}. \tag{4}$$

Similar to Ref. [79], the absolute MR effect (A_{MR}) and the relative MR effect (R_{MR}) are defined as

$$A_{\mathrm{MR}} = \left|G^*_{\mathrm{B=0.51\ T}}\right| - \left|G^*_{\mathrm{B=0\ T}}\right|, \tag{5}$$

and

$$R_{\mathrm{MR}} = \frac{\left|G^*_{\mathrm{B=0.51\ T}}\right| - \left|G^*_{\mathrm{B=0\ T}}\right|}{\left|G^*_{\mathrm{B=0\ T}}\right|}, \tag{6}$$

where $\left|G^*_{\mathrm{B=0.51\ T}}\right|$ and $\left|G^*_{\mathrm{B=0\ T}}\right|$ represents the magnitude of shear modulus at 0.51 T and 0 T, respectively. In this manuscript, the analysis of the measurement data and the figures is carried out using MATLAB (Release 2020b, The MathWorks, Inc., Natick, Massachusetts, United States).

3. Measurement of static and dynamic mechanical properties

For the static mechanical test, triangle wave shear deformation with an amplitude of 0.3 mm (corresponding to 15% simple shear strain) was applied to the MRE samples. According to Refs. [80–82], initially, three kinds of strain rate which are 0.008 s^{-1}, 0.002 s^{-1} and 0.0005 s^{-1}, respectively, are applied to the ANI-VP MRE sample without magnetic field. The change of shear force with respect to time is shown in Fig. 6. It can be found that the decrease of the maximum shear force from 0.002 s^{-1} to 0.0005 s^{-1} is much smaller compared with that from 0.008 s^{-1} to 0.002 s^{-1} strain rate. Considering that there is a shape increase in temperature caused by the long term working of the two

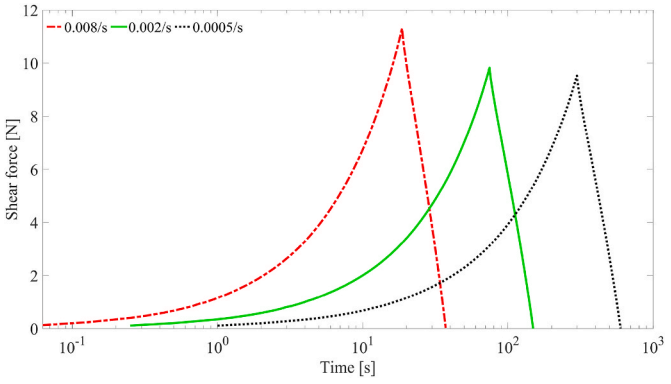

Fig. 6. Time-force curve (for ease of viewing, a logarithmic coordinate is used for the x-axis) for the ANI-PV MRE sample under different strain loading rates without magnetic field.

electromagnets at 0.0005 s^{-1} strain loading rate, the final strain rate for the static test is set to be 0.002 s^{-1} and the corresponding sampling frequency is set to be 4 Hz.

During static measurement, the applied magnetic field varied from 0 to 0.51 T with an interval of 0.17 T. The stress-strain curves for anisotropic MRE with different particle chain-magnetic field spatial locations are shown in Fig. 7. By comparing major axis slopes of the different anisotropic MRE samples, it can be found that the order of increasing shear modulus magnitude for MRE is ANI-PV, ANI-VV, ANI-VP and ANI-PP. Physically, a large MR effect is exhibited for the ANI-PV MRE sample since the particles within the sample are mainly distributed along the direction of the magnetic field and easier to be magnetized compared with other anisotropic MRE samples. Furthermore, the presence of the MR effect for the ANI-VP and the ANI-VV MRE sample demonstrate that by applying a magnetic field during the curing stage cannot guarantee that all iron particles are totally distributed along the same direction. Interestingly, the shear stresses for the ANI-VV and the ANI-PP MRE samples keep constant when the applied magnetic field is larger than 0.34 T compared with the continuous increase of the shear stress for the ANI-PV and the ANI-VP MRE samples. As proved in the appendix, the Maxwell stress tensors, $2\Omega_5\gamma H^2 + 2\Omega_{10}\gamma H$ and $2\Omega_5\gamma H^2$, respectively, contribute to the total shear stress for the ANI-PV and the ANI-VP MRE samples. On the contrary, only mechanical stresses, $2\Omega_1\gamma + 2\Omega_7\gamma$ and $2\Omega_1\gamma$ contribute to the total shear stress for the ANI-VV and the ANI-PP MRE sample. Since the saturation magnetization strength for the anisotropic MRE samples is 0.3873 T, the stress strain curves for the ANI-VV and the ANI-PP MRE samples at 0.34 T and 0.51 T overlap. Despite the magnetic saturation, the magnetic saturation of the MRE does not hinder the growth of the internal magnetic field strength (H). Therefore, the shear stress continues to increase after 0.34 T for the ANI-PV and the ANI-VP MRE samples. So far, the authors have not found any similar report to the above mentioned experimental phenomenon from other literatures. Moreover, the enclosed non-zero areas of the stress-strain hysteresis loop by the different anisotropic MRE samples indicate that even under quasi-static condition, the MRE sample nevertheless present an inelastic behavior.

To characterize the dynamic mechanical behavior of the above mentioned MRE samples, the strain amplitude (3%, 6%, 9% and 12%), magnetic field strength (0, 0.17, 0.34 and 0.51 T) and the frequency (1, 3, 6, 9, 12, 18 and 21 Hz) were varied during the measurements. All combinations of the strain amplitude, magnetic field strength and frequency were measured, recorded over 20 periods, and the sampling frequency was set to be 1000 Hz. Only the data corresponding to 9%, 6% and 3% dynamic strain amplitude are used for the subsequent analysis. The 12% dynamic strain is used to fully remove the Mullins effect from the test result. After applying the Fourier transformation of the stress and strain as shown in Eq. (2), the equivalent shear modulus magnitude and loss factor in frequency domain under different magnetic fields and strain amplitudes can be obtained. The comparisons of the equivalent shear modulus magnitude and loss factor of the different MRE samples under different strain amplitudes are shown in Figs. 8–10. Clearly, there is an obvious MR effect for all the four test samples. Taking the shear modulus of the different MRE samples under 1 Hz and 3% dynamic strain amplitude as an example, the absolute MR effects are 0.2417 MPa, 0.0568 MPa, 0.0594 MPa and 0.0730 MPa for the ANI-PV, ANI-VV, ANI-VP and the ANI-PP MRE samples, whereas the corresponding relative MR effects are 107.87%, 24.79%, 36.83% and 56.92%, respectively.

In addition to the influence of the shear modulus, it can be found that the magnetic field also influences the loss factor of the MRE samples. Specifically, the loss factor increases slightly with increasing magnetic field for the ANI-VP and the ANI-PP MRE samples, while it increases significantly with increasing magnetic field for the ANI-PV and the ANI-VV MRE samples. Physically, the sharp increase of the loss factor for the ANI-PV and the ANI-VV MRE samples could be related to the increases interface interaction between particles and matrix after applying the magnetic field.

Moreover, as shown in Figs. 8–10, there is a frequency dependence of the dynamic shear modulus of the MRE samples. In specific, the magnitude and loss factor of the shear modulus of the tested anisotropic MRE samples increase with increasing frequency. The shear modulus magnitude of the different MRE samples under 1 Hz and 21 Hz are shown in Table 1. It can be found that there is an evident Payne effect [83] of the dynamic shear modulus of the MRE samples additional to the frequency dependency of the dynamic shear modulus. In specific, the shear modulus magnitude decreases with increasing strain amplitude during cyclic oscillation. Furthermore, as shown in Figs. 7–9, it can be found that the loss factor of the ANI-PV and the ANI-VV MRE samples is slightly larger than that of the ANI-VP and the ANI-PP MRE samples, which demonstrate that the loss factor of anisotropic MRE with different particle chain-deformation field spatial location is totally different. Physically, there is no stretch for particle chains in the ANI-VP and the ANI-PP MRE samples, while a stretch is exhibited for the ANI-PV and the

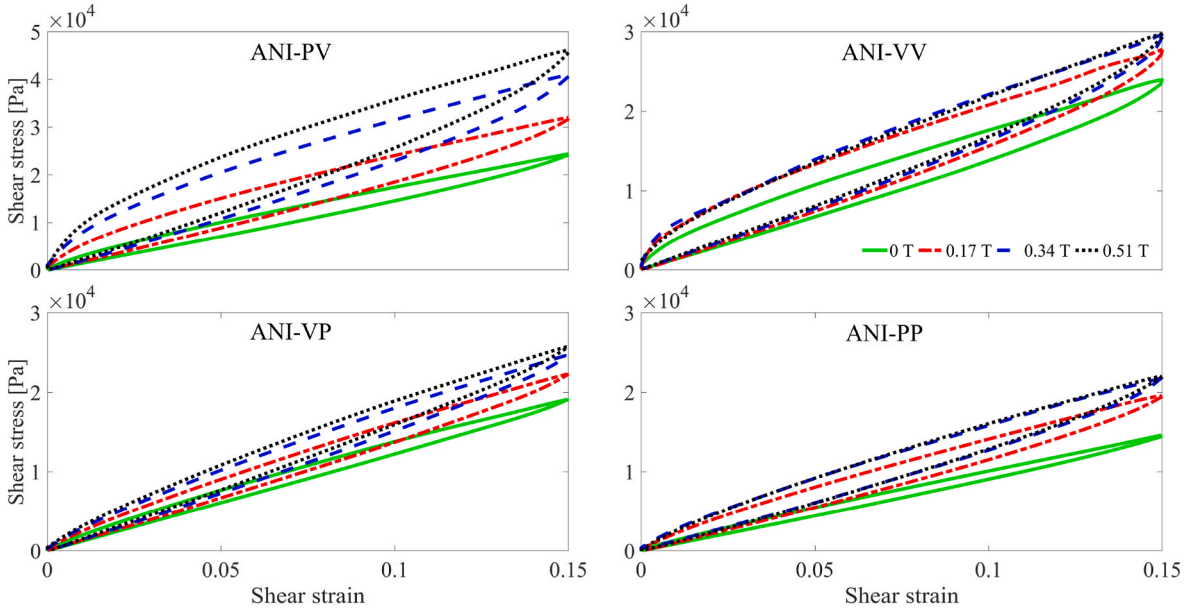

Fig. 7. Static hysteresis loops for anisotropic MRE sample with different particle chain-magnetic field spatial location.

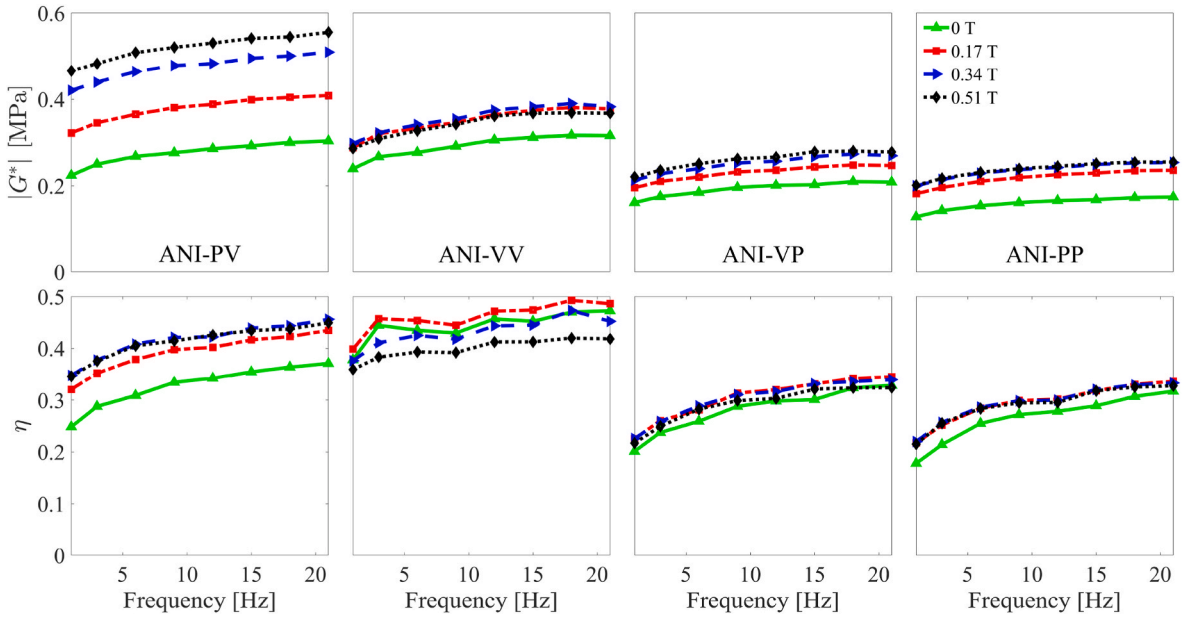

Fig. 8. The magnitude and loss factor of the shear modulus versus frequency of the different MRE samples (ANI-PV, ANI-VV, ANI-VP and the ANI-PP) at 3% strain amplitude under different magnetic field strengths.

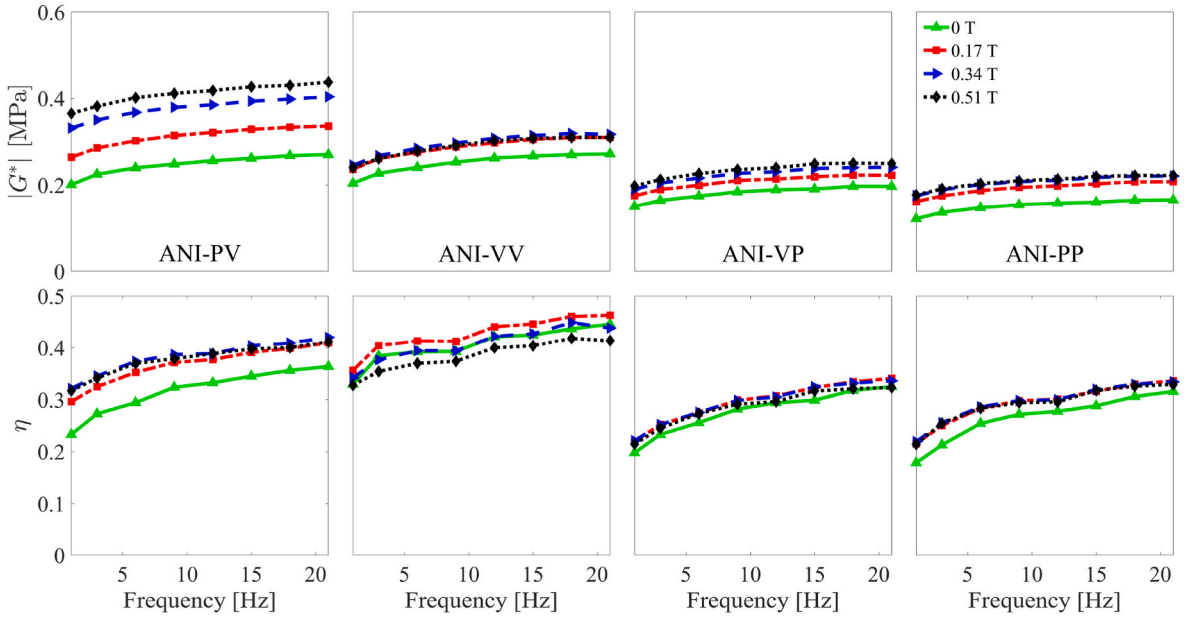

Fig. 9. The magnitude and loss factor of the shear modulus versus frequency of the different MRE samples (ANI-PV, ANI-VV, ANI-VP and the ANI-PP) at 6% strain amplitude under different magnetic field strengths.

ANI-VV MRE samples under simple shear deformation. Therefore, a stronger interaction between aligned particles and matrix is encountered for the ANI-PV and the ANI-VV MRE samples, leading to a larger loss factor.

Through the measurement results in Figs. 7–10, it can be seen that the mechanical performance of anisotropic MREs is strongly dependent on the coupling among the spatial location of particle chains, the direction of the magnetic field applied and the direction of the deformation applied. In order to obtain a higher MR effect, it is recommended that the iron particles are distributed in chains and in parallel with the external magnetic field. However, the presence of the MR effect for anisotropic MRE where the column like structures of iron particles are in perpendicular to the magnetic field indicates that the application of a magnetic field cannot insure that all iron particles are completely distributed along the applied magnetic field direction. Therefore, in perspective of constitutive modeling of the mechanical performance of anisotropic MRE, besides the contribution of the anisotropic part (particle chain induced anisotropy), the fundamental contribution of the isotropic part should be taken into account primarily. Furthermore, the difference of the stress-strain hysteresis loops for anisotropic MRE samples with different particle chain-magnetic field spatial locations under 0.34 and 0.51 T indicates that Maxwell stress tensor, which represents the interaction between electromagnetic forces and mechanical momentum also contributes to the MR effect of MRE.

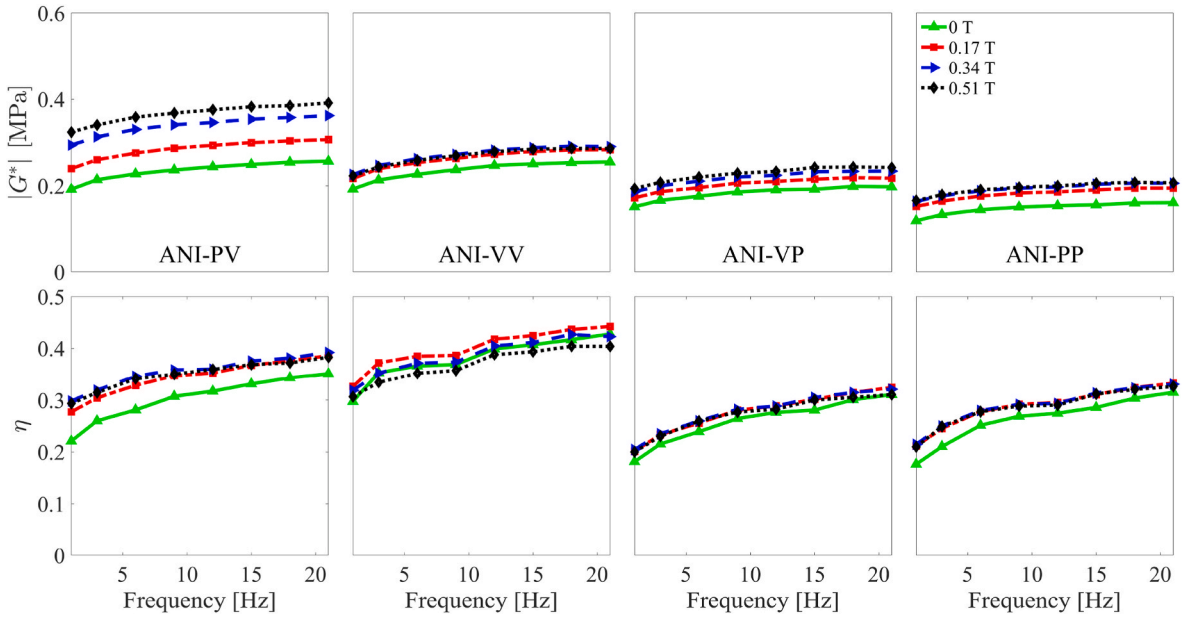

Fig. 10. The magnitude and loss factor of the shear modulus versus frequency of the different MRE samples (ANI-PV, ANI-VV, ANI-VP and the ANI-PP) at 9% strain amplitude under different magnetic field strengths.

Table 1
The equivalent dynamic shear modulus magnitude for different MRE samples at 1 and 21 Hz under 0 and 0.51 T.

$\lvert G^*(\omega)\rvert$ [MPa]		ANI-PV		ANI-VV		ANI-VP		ANI-PP	
Frequency	Amplitude	0 T	0.51 T	0 T	0.51 T	0 T	0.51 T	0 T	0.51 T
1 Hz	9%	0.1919	0.3237	0.1923	0.2230	0.1514	0.1937	0.1192	0.1659
	3%	0.2241	0.4658	0.2393	0.2862	0.1611	0.2205	0.1282	0.2011
21 Hz	9%	0.2568	0.3913	0.2550	0.2865	0.1975	0.2421	0.1610	0.2071
	3%	0.3036	0.5554	0.3159	0.3676	0.2085	0.2782	0.1740	0.2549

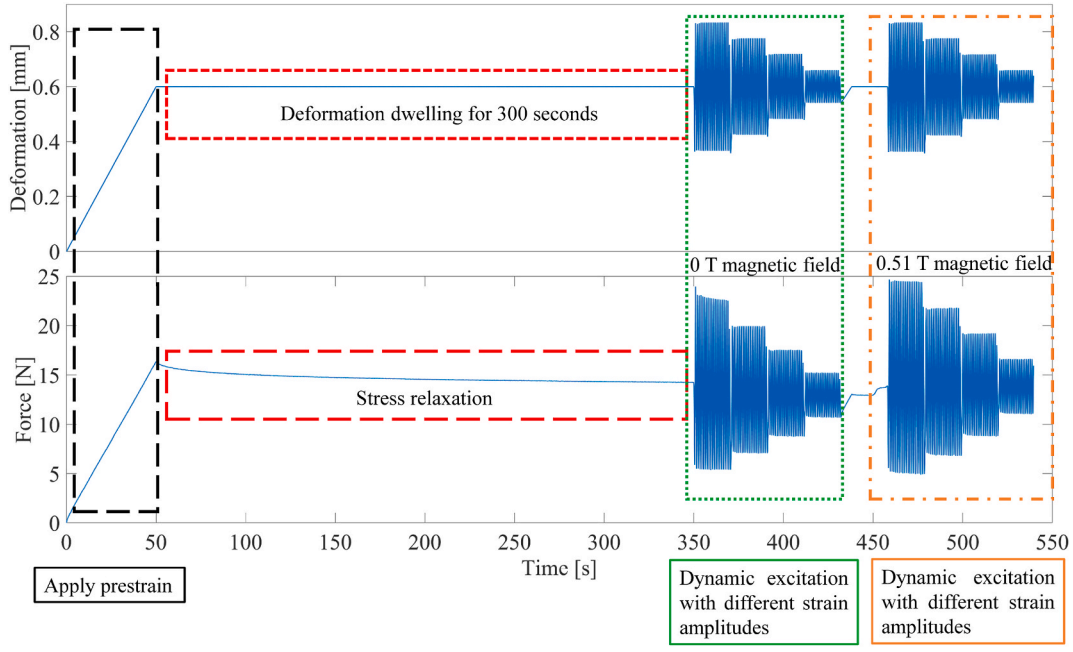

Fig. 11. Prescribed loading as a function of time and the stress response.

4. Measurement of dynamic mechanical properties under prestrain

In practical applications, especially applications in the field of vibration control, static prestrain caused by the target structure is often encountered [84,85]. The prestrain will change the mechanical behavior of MREs, thereby affecting the vibration control effect. In order to analyze the effect of prestrain on the mechanical properties of anisotropic MRE, characterization of the dynamic performance of anisotropic MRE samples as shown in Fig. 1 under 30% and 60% prestrain at 0 and 0.51 T magnetic field was conducted after having tested the dynamic performance of the MRE samples without prestrain. To compensate the effect of stress relaxation, the loading condition shown in Fig. 11 was applied. Firstly, a prestrain with a strain rate of 0.01 s^{-1} was applied. After finishing the prestrain, the prestrained sample is dwelled for 300 s to fully complete the stress relaxation process. Subsequently, dynamic strain with amplitudes of 12%, 9%, 6% and 3% at 0 and 0.51 T was applied sequentially. As mentioned previously, only data corresponding to 9%, 6% and 3% dynamic strain amplitude are used. The dynamic strain with an amplitude of 12% is used to fully offset the Mullins effect on the test result.

To analyze the influence of prestrain on the dynamic mechanical performance of MRE, the stress-strain hysteresis loops for the above mentioned four kinds of test settings under 1 Hz at different magnetic fields (0 and 0.51 T) and different prestrains (0%, 30% and 60%) with a 3% dynamic strain amplitude were studied, as shown in Figs. 12 and 13. In order to facilitate the comparison of the stress-strain results under different prestrains, the static force part caused by the prestrain is erased and only the dynamic force part is shown in Figs. 12 and 13. By comparing the peak-to-valley stress value at 0 and 0.51 T under different prestrains, it can be found that there is an MR effect for the different anisotropic MRE samples even with prestrain. Furthermore, the curves under 60% prestrain are constantly stiffer than the corresponding curves without prestrain at 0 T, while the curves under 30% prestrain at 0 T seem to be close to the corresponding curves without any prestrain.

After applying the Fourier transform-based method in Eq. (2), the equivalent shear modulus magnitudes of the ANI-PV, ANI-VV, ANI-VP and the ANI-PP MRE samples at 1Hz and 3% dynamic strain amplitude with different prestrains at 0 and 0.51 T are obtained in Table 2. Clearly, the relative MR effects of the MRE samples gradually decrease as the prestrain increases. Compared with the ANI-VV, ANI-VP and the ANI-PP MRE samples, the MR effect of the ANI-PV MRE sample is more affected by the prestrain, with a sharp decrease of the MR effect (from 107.83% to 39.83%) with the prestrain increase (from 0% to 60%). Therefore, from an engineering applications perspective, a deep study of the influence of prestrain on the MR effect is needed in order to guarantee safety and reliability while utilizing the anisotropic MRE with prestrain.

In order to analyze the effect of prestrain on the dynamic mechanical behavior of MRE thoroughly, the results for the magnitude and the loss factor of the equivalent shear modulus of the different MRE samples with different prestrains and frequencies are shown in Figs. 14–16. It can be found that the prestrain also affects the loss factor of the MRE samples besides the influence on the modulus magnitude. Specifically, the loss factor decreases with increasing prestrain. Although the effect of prestrain and magnetic field on the magnitude of the equivalent shear modulus of MRE is similar, with increasing magnitude for increasing prestrain and increasing magnetic field. The effect of prestrain and magnetic field on the loss factor is the opposite; namely, a larger prestrain leads to a smaller value of the loss factor, while a higher magnetic field leads to a larger value of the loss factor.

Furthermore, it can be found that the prestrain also influences the frequency dependency of the MRE samples. Without prestrain, the shear modulus magnitude monotonically increases from 1 to 21 Hz. However, under prestrain, the increasing trend of the shear modulus magnitude with respect to frequency reaches a plateau. A possible explanation for the decline of the frequency dependency with applied prestrain is the crystallinity of the rubber matrix along the direction of prestrain. According to Ref. [84], rubber materials display a preferred chain alignment in the prestrained direction and eventually crystallinity will be induced. Compared with the glassy state, a high elasticity will be present after strain induced crystallization leading to a less pronounced frequency dependency and a smaller value of loss factor. Moreover, as can be noted in Figs. 14–16, the shear modulus magnitude decreases slightly at 18 and 21 Hz for the ANI-PV, ANI-VV and the ANI-VP samples under 60% prestrain. During the measurement, there was an obvious vibration accompanied by a rhythmic sound of the extension rod which connects the electromagnetic motor 1 and the shear fixture for the DMA machine at 18 and 21 Hz. Therefore, a possible explanation for this abnormal phenomena is the resonance of the whole test system.

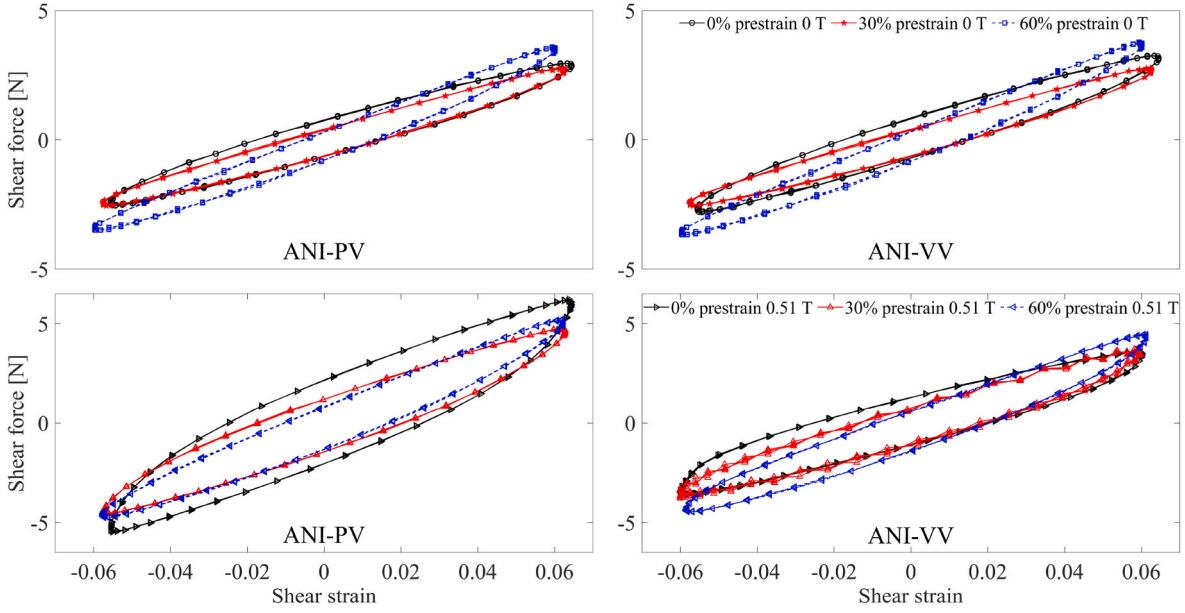

Fig. 12. Stress-strain hysteresis curves of the ANI-PV and the ANI-VV MRE samples under different prestrains (0%, 30% and 60%) and magnetic fields (0 and 0.51 T).

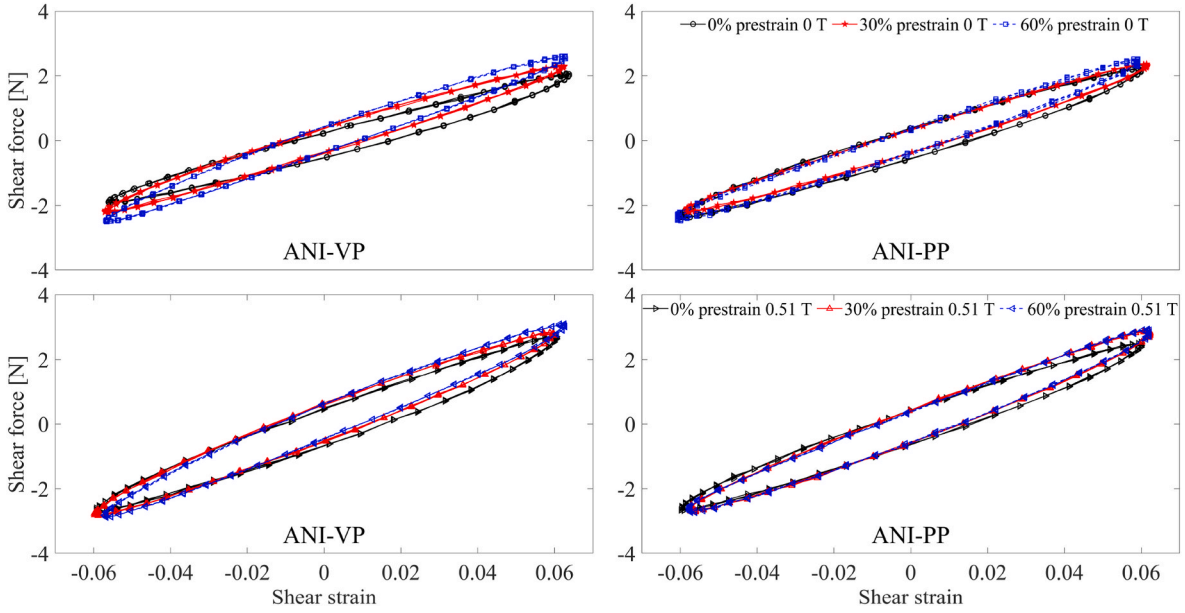

Fig. 13. Stress-strain hysteresis curves of the ANI-VP and the ANI-PP MRE samples under different prestrains (0%, 30% and 60%) and magnetic fields (0 and 0.51 T).

Table 2
The equivalent shear modulus magnitude and the relative MR effect of the different MRE samples at different prestrains and magnetic fields.

Prestrain and magnetic field		ANI-PV		ANI-VV		ANI-VP		ANI-PP	
		$\|G^*\|$ [MPa]	R_{MR}	$\|G^*\|$ [MPa]	R_{MR}	$\|G^*\|$ [MPa]	R_{MR}	$\|G^*\|$ [MPa]	R_{MR}
0%	0 T	0.2241	107.83%	0.2393	19.60%	0.1611	36.83%	0.1282	56.86%
	0.51 T	0.4658		0.2862		0.2205		0.2011	
30%	0 T	0.2171	73.92%	0.2455	20.04%	0.1863	24.75%	0.1316	44.68%
	0.51 T	0.3777		0.2947		0.2324		0.1904	
60%	0 T	0.2908	39.83%	0.2380	21.01%	0.2105	16.29%	0.1457	28.21%
	0.51 T	0.4067		0.2880		0.2448		0.1868	

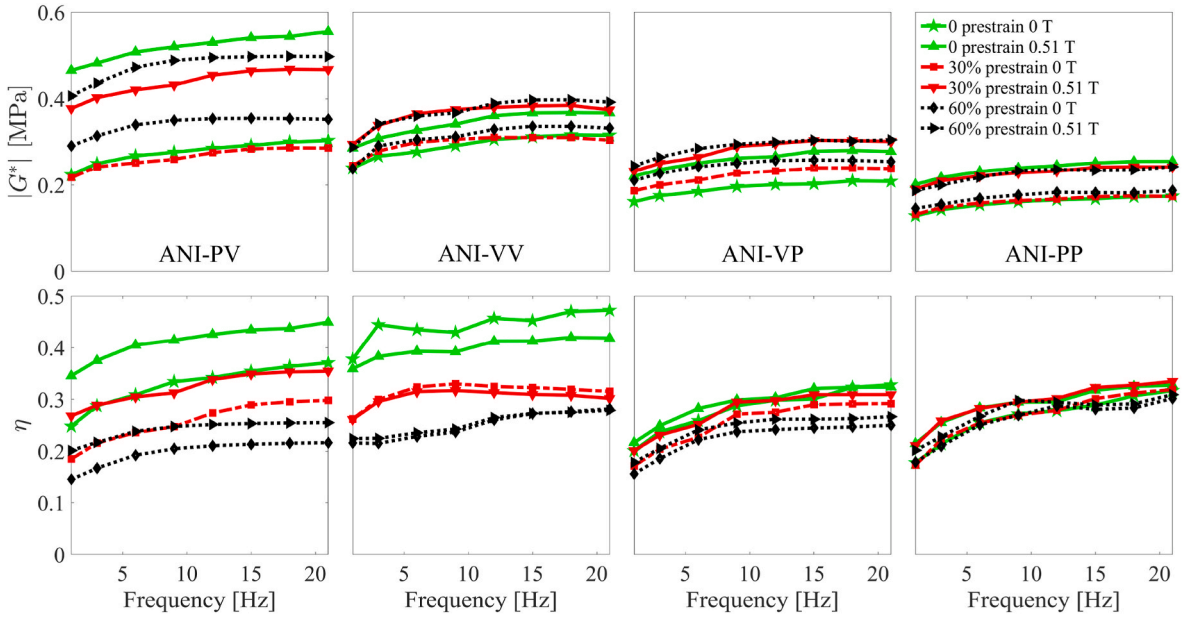

Fig. 14. The magnitude and loss factor of shear modulus of the different MRE samples (ANI-PV, ANI-VV, ANI-VP and ANI-PV) at 3% dynamic strain amplitude with different prestrains and magnetic fields.

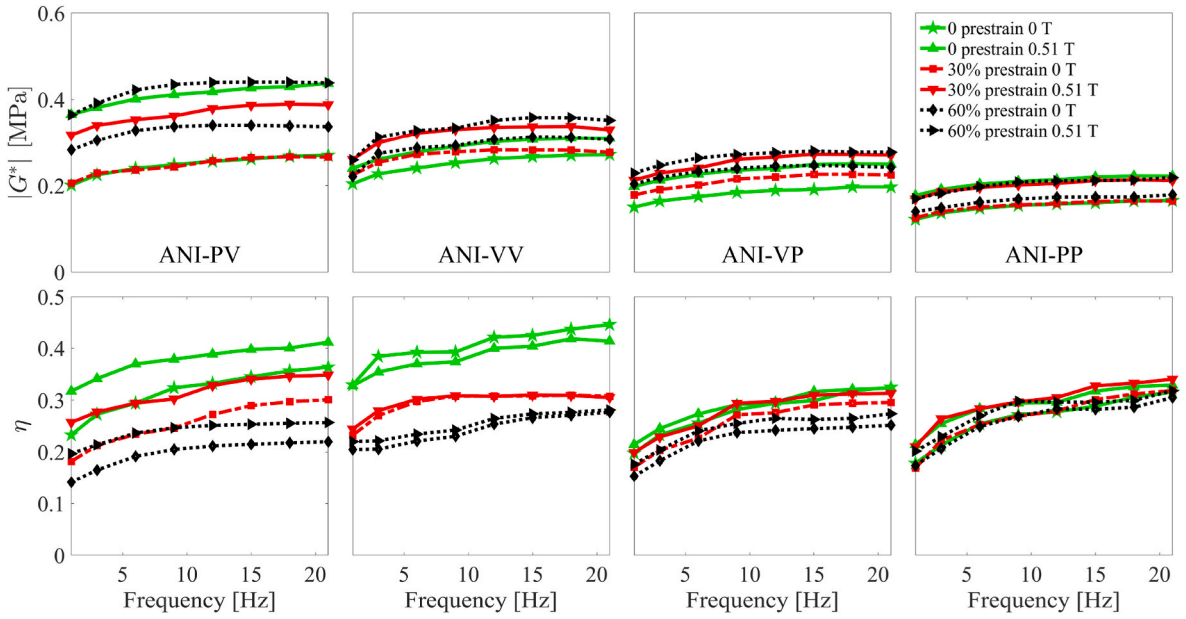

Fig. 15. The magnitude and loss factor of shear modulus of the different MRE samples (ANI-PV, ANI-VV, ANI-VP and ANI-PV) at 6% dynamic strain amplitude with different prestrains and magnetic fields.

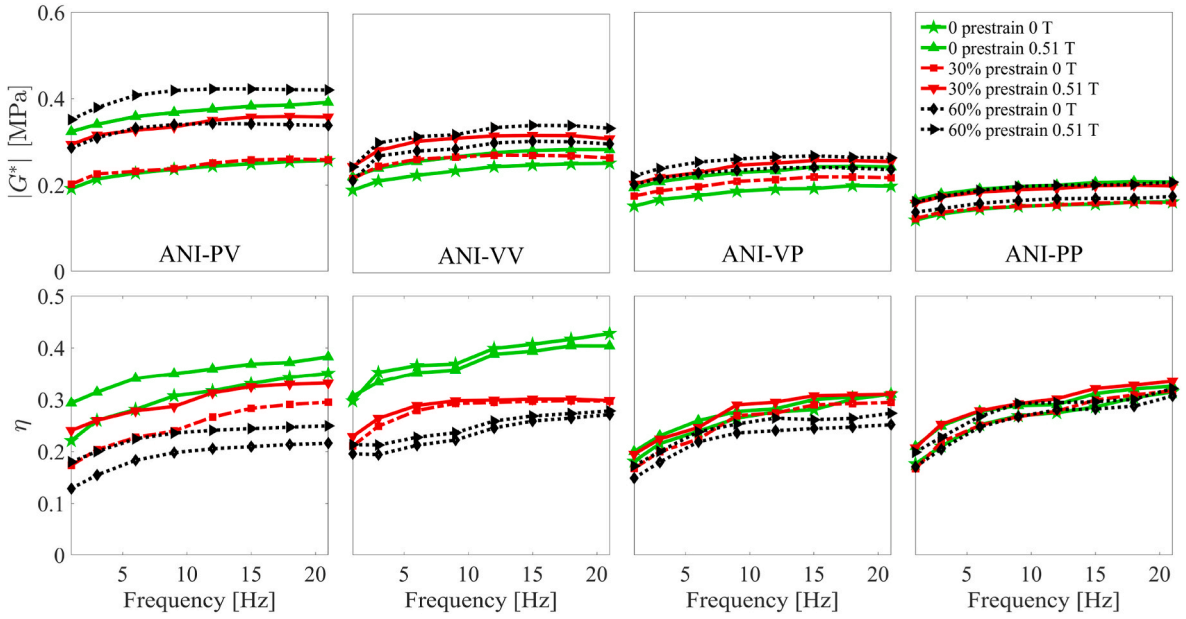

Fig. 16. The magnitude and loss factor of shear modulus of the different MRE samples (ANI-PV, ANI-VV, ANI-VP and ANI-PV) at 9% dynamic strain amplitude with different prestrains and magnetic fields.

5. Conclusion and outlook

This investigation covers a broad magneto-mechanical characterization of MRE. Based on the test, the following conclusions are obtained:

- All the four types of MREs (ANI-PV, ANI-VV, ANI-VP and the ANI-PP MRE) exhibit an obvious MR effect. Since most particle chains within the ANI-PV MRE are parallel to the direction of the applied magnetic field, the MR effect is the largest for ANI-PV MRE among the four tested samples. Furthermore, besides the interaction of the adjacent particles after magnetization, Maxwell stress tensor contributes to the MR effect of MRE as well.
- Regarding the dynamic mechanical performance, the dynamic shear modulus magnitude increases with increased frequency and decreases with increased strain amplitude for the four kinds of MRE samples. In addition to the influence on the dynamic shear modulus magnitude, the magnetic field affects the loss factor of MRE as well. In specific, the loss factor increases slightly with increased magnetic field for the ANI-VP and the ANI-PP MRE samples, while the loss factor of the ANI-PV and the ANI-VV MRE samples increases significantly with the increase of the magnetic field.
- Compared with the magnetic field, the effect of the prestrain on the dynamic behavior of MRE is more complicated. Even though the shear modulus magnitudes of the tested MRE samples is larger under 60% prestrain compared to those without prestrain at 0T, the MR

effect gradually decrease as the prestrain increases. Besides, the loss factor and the frequency dependency of the MRE samples gradually decrease as the increase of the prestrain.

The characterization of the magneto-mechanical performance of the MREs presented in this study promotes the application and constitutive modeling of MRE. In the near future, a constitutive model which reflects the influence of frequency, strain amplitude and magnetic field on the magneto-mechanical behavior of anisotropic MRE is expected to be developed.

Data availability statement

The raw/processed data required to reproduce these findings cannot be shared at this time as the data also forms part of an ongoing study.

CRediT authorship contribution statement

Bochao Wang: Investigation, Formal analysis, Validation, Writing – original draft, Methodology, Visualization, Writing – review & editing. **Yan Li:** Investigation, Validation, Methodology, Visualization. **Yingduan Gao:** Investigation, Methodology. **Jingyi Zhang:** Investigation, Methodology. **Zhenbang Xu:** Writing – review & editing. **Jun Li:** Investigation, Methodology. **Ji Li:** Investigation, Methodology. **Leif Kari:** Supervision, Project administration, Writing – review & editing. **Yu Wang:** Supervision, Project administration. **Xinglong Gong:** Resources, Supervision, Project administration, Funding acquisition.

Declaration of competing interest

The authors declare that they have no known competing financial interests or personal relationships that could have appeared to influence the work reported in this paper.

Acknowledgements

Financial supports from the National Natural Science Foundation of China (11972343, 12132016), the Anhui Key R&D Program of China (202104a05020009) and the Fundamental Research Funds for the Central Universities (WK2090000030) are gratefully acknowledged. Furthermore, the proofreading by Maria Del Mar Vizcaino Vergara is highly appreciated.

APPENDIX

Appendix. Derivation of the shear stress for anisotropic MREs with different particle chain-magnetic-deformation spatial locations

For classical transversely isotropic material, normally, two kind of loading conditions such as simple shear where the direction of the deformation is axial and transverse to the isotropy plane are sufficient to extract the representative material parameters. Even though the MRE investigated in this manuscript has only one preferred direction and should be classified as transversely isotropic material, due to the strong coupling among the magnetic field, the deformation field and the particle chain like structure, there is a significant different between the MRE in this study and the classical transversely isotropic material. Following the path of Ref. [47], the direction of the column like structure of the carbonyl iron particles in the reference configuration is denoted by a unit vector$\mathbf{a}_0$. The direction of the column like structure of the carbonyl iron particles in Fig. 1 are

$$\mathbf{a}_{0\mathrm{ANI-PV}} = \mathbf{a}_{0\mathrm{ANI-VV}} = \begin{bmatrix} 1 \\ 0 \\ 0 \end{bmatrix} \tag{A.1}$$

and

$$\mathbf{a}_{0\mathrm{ANI-VP}} = \mathbf{a}_{0\mathrm{ANI-PP}} = \begin{bmatrix} 0 \\ 0 \\ 1 \end{bmatrix}. \tag{A.2}$$

By applying the continuous condition of the normal component of the magnetic field vector, it can be obtained that the magnetic field vector inside MRE are

$$\mathbf{H}_{0\mathrm{ANI-PV}} = \mathbf{H}_{0\mathrm{ANI-VP}} = \begin{bmatrix} H_1 \\ 0 \\ 0 \end{bmatrix} \tag{A.3}$$

and

$$\mathbf{H}_{0\mathrm{ANI-VV}} = \mathbf{H}_{0\mathrm{ANI-PP}} = \begin{bmatrix} 0 \\ 0 \\ H_3 \end{bmatrix}, \tag{A.4}$$

where H_1 and H_3 are variables need to be determined by the constitutive model. Combing with Eq. (1), the left Caucy-Green deformation tensor is

$$\mathbf{b} = \mathbf{F}\mathbf{F}^{\mathrm{T}} = \begin{bmatrix} 1 & \gamma & 0 \\ \gamma & 1+\gamma^2 & 0 \\ 0 & 0 & 1 \end{bmatrix} \tag{A.5}$$

By applying Eq. (84) in Ref. [47] and only consider the deviatoric stress, it can be obtained that

$$\boldsymbol{\tau} = 2\mathbf{b}\Omega_1 + 2\mathbf{b}\mathbf{H} \otimes \mathbf{b}\mathbf{H}\Omega_5 + 2(\mathbf{F}\mathbf{a}_0) \otimes (\mathbf{F}\mathbf{a}_0)\Omega_7 + [(\mathbf{F}\mathbf{a}_0) \otimes \mathbf{b}\mathbf{H} + \mathbf{b}\mathbf{H} \otimes (\mathbf{F}\mathbf{a}_0)]\Omega_{10}, \tag{A.6}$$

where Ω_i is the derivative of Ω with respect to the ith tensor invariant and Ω_i can be viewed as the parameters needed to identified. Inserting Eqs. (1,

A.1-5) into Eq. (A.6), it can be obtained that the shear stress for the four kinds of test settings in Fig. 1 are

$$\tau_{\mathrm{ANI-PV}} = 2\Omega_1\gamma + 2\Omega_5\gamma H_1^2 + 2\Omega_7\gamma + 2\Omega_{10}\gamma H_1, \tag{A.7}$$

$$\tau_{\mathrm{ANI-VP}} = 2\Omega_1\gamma + 2\Omega_5\gamma H_1^2, \tag{A.8}$$

$$\tau_{\mathrm{ANI-VV}} = 2\Omega_1\gamma + 2\Omega_7\gamma \tag{A.9}$$

and

$$\tau_{\mathrm{ANI-PP}} = 2\Omega_1\gamma, \tag{A.10}$$

where Ω_i represents the partial derivative of the modified free energy Ω with respect to the tensor invariants I_i. Specifically, Ω_1 and Ω_7 stand for the contribution of the magneto-mechanical stress, while Ω_5 and Ω_{10} are the contribution of the Maxwell stress to the total Cauchy stress. For more details, please check Refer [47]. Even though the mechanical performance of MRE is not pure hyperelastic, the hyperelastic stress solution in Eqs. (A.7) to (A.10) play a fundamental role to guide the characterization of the mechanical behavior of anisotropic MRE. Since there are four unknowns (Ω_1, Ω_5, Ω_7 and Ω_{10}) in Eqs. (A.7) to (A.10), four kinds of test settings as shown in Fig. 1 are needed for the completeness of the characterization of the magneto-elastic performance and the identification of the material parameters for the constitutive model developed of anisotropic MRE.

References

[1] S. Bahl, H. Nagar, I. Singh, S. Sehgal, Smart materials types, properties and applications: a review, Mater Today: SAVE Proc. 28 (2020) 1302–1306.
[2] A.K. Bastola, M. Paudel, L. Li, W. Li, Recent progress of magnetorheological elastomers: a review, Smart Mater. Struct. 29 (2020) 123002.
[3] Q. Wen, L. Shen, J. Li, S. Xuan, Z. Li, X. Fan, et al., Temperature dependent magneto-mechanical properties of magnetorheological elastomers, J. Magn. Magn Mater. 497 (2020) 165998.
[4] C. Sun, X. Cao, X. Zhou, X. Gong, S. Xuan, Deformation dependent sound absorption property of a novel magnetorheological membrane sound absorber, Front Mater 7 (2020) 375.
[5] X. Cao, S. Xuan, J. Li, Z. Li, T. Hu, H. Liang, et al., Magnetic-tunable sound absorber based on micro-perforated magnetorheological elastomer, Smart Mater. Struct. 29 (1) (2019), 015024.
[6] G. Liao, X. Gong, S. Xuan, Phase based stiffness tuning algorithm for a magnetorheological elastomer dynamic vibration absorber, Smart Mater. Struct. 23 (1) (2013), 015016.
[7] Y. Bian, X. Liang, Z. Gao, Vibration reduction for a flexible arm using magnetorheological elastomer vibration absorber, Shock Vib (2018) 9723538.
[8] W. Li, X. Zhang, H. Du, Development and simulation evaluation of a magnetorheological elastomer isolator for seat vibration control, J. Intell. Mater. Syst. Struct. 23 (9) (2012) 1041–1048.
[9] Y. Li, J. Li, W. Li, B. Samali, Development and characterization of a magnetorheological elastomer based adaptive seismic isolator, Smart Mater. Struct. 22 (3) (2013), 035005.
[10] H.-J. Jung, S.-H. Eem, D.-D. Jang, J.-H. Koo, Seismic performance analysis of a smart base-isolation system considering dynamics of MR elastomers, J. Intell. Mater. Syst. Struct. 22 (13) (2011) 1439–1450.
[11] Z. Xing, M. Yu, J. Fu, Y. Wang, L. Zhao, A laminated magnetorheological elastomer bearing prototype for seismic mitigation of bridge superstructures, J. Intell. Mater. Syst. Struct. 26 (14) (2015) 1818–1825.
[12] Q. Wang, X. Dong, L. Li, J. Ou, Mechanical modeling for magnetorheological elastomer isolators based on constitutive equations and electromagnetic analysis, Smart Mater. Struct. 27 (6) (2018), 065017.
[13] B. Wang, T. Hu, L. Shen, J. Li, Z. Xu, L. Kari, et al., Magneto-sensitive rubber in a vehicle application context-exploring the potential, Front Mater 8 (2021) 150.
[14] E. Rustighi, D.F. Ledezma-Ramirez, P.E. Tapia-Gonzalez, N. Ferguson, A. Zakaria, Modelling and experimental characterisation of a compressional adaptive magnetorheological elastomer isolator, J. Vib. Control (2021), 10775463211025336.
[15] A. Alberdi-Muniain, N. Gil-Negrete, L. Kari, Modelling energy flow through magneto-sensitive vibration isolators, Int. J. Eng. Sci. 65 (2013) 22–39.
[16] A. Alberdi-Muniain, N. Gil-Negrete, L. Kari, Indirect energy flow measurement in magneto-sensitive vibration isolator systems, Appl. Acoust. 74 (4) (2013) 575–584.
[17] A. Alberdi-Muniain, N. Gil-Negrete, L. Kari, Direct energy flow measurement in magneto-sensitive vibration isolator systems, J. Sound Vib. 331 (9) (2012) 1994–2006.
[18] Q. Zhang, B. Peng, H. Li, J. Sun, Magnetically tunable transparency for magnetorheological elastomer films consisting of polydimethylsiloxane and Fe3O4 nanoparticles, Soft Mater 16 (3) (2018) 220–227.
[19] J.-H. Koo, A. Dawson, H.-J. Jung, Characterization of actuation properties of magnetorheological elastomers with embedded hard magnetic particles, J. Intell. Mater. Syst. Struct. 23 (9) (2012) 1049–1054.
[20] X. Kuang, S. Wu, Y. Jin, Q. Ze, S.M. Montgomery, L. Yue, et al., Magnetic dynamic polymers for modular assembling and reconfigurable morphing architectures, Adv. Mater. (2021) 2102113.
[21] Y. Kim, G.A. Parada, S. Liu, X. Zhao, Ferromagnetic soft continuum robots, Sci Robot 4 (33) (2019).
[22] C. Wu, Q. Zhang, X. Fan, Y. Song, Q. Zheng, Smart magnetorheological elastomer peristaltic pump, J. Intell. Mater. Syst. Struct. 30 (7) (2019) 1084–1093.
[23] E. Psarra, L. Bodelot, K. Danas, Two-field surface pattern control via marginally stable magnetorheological elastomers, Soft Matter 13 (37) (2017) 6576–6584.
[24] E. Psarra, L. Bodelot, K. Danas, Wrinkling to crinkling transitions and curvature localization in a magnetoelastic film bonded to a non-magnetic substrate, J. Mech. Phys. Solid. 133 (2019) 103734.
[25] L. Ding, S. Xuan, J. Feng, X. Gong, Magnetic/conductive composite fibre: a multifunctional strain sensor with magnetically driven property, Composer Part A Appl Sci Manuf 100 (2017) 97–105.
[26] Q. Shu, T. Hu, Z. Xu, J. Zhang, X. Fan, X. Gong, et al., Non-tensile piezoresistive sensor based on coaxial fiber with magnetoactive shell and conductive flax core, Composer Part A Appl Sci Manuf (2021) 106548.
[27] T. Hu, S. Xuan, L. Ding, X. Gong, Liquid metal circuit based magnetoresistive strain sensor with discriminating magnetic and mechanical sensitivity, Sensor. Actuator. B Chem. 314 (2020) 128095.
[28] M.R. Jolly, J.D. Carlson, B.C. Munoz, A model of the behaviour of magnetorheological materials, Smart Mater. Struct. 5 (5) (1996) 607.
[29] L. Chen, X. Gong, W. Li, Microstructures and viscoelastic properties of anisotropic magnetorheological elastomers, Smart Mater. Struct. 16 (6) (2007) 2645.
[30] Y. Zhu, X. Gong, H. Dang, X. Zhang, P. Zhang, Numerical analysis on magnetic-induced shear modulus of magnetorheological elastomers based on multi-chain model, Chin. J. Chem. Phys. 19 (2) (2006) 126–130.
[31] D. Garcia-Gonzalez, M. Hossain, Microstructural modelling of hard-magnetic soft materials: dipole–dipole interactions versus Zeeman effect, Extreme Mech Lett (2021) 101382.
[32] Y. Han, W. Hong, L.E. Faidley, Field-stiffening effect of magneto-rheological elastomers, Int. J. Solid Struct. 50 (14–15) (2013) 2281–2288.
[33] D. Ivaneyko, V. Toshchevikov, M. Saphiannikova, G. Heinrich, Mechanical properties of magneto-sensitive elastomers: unification of the continuum-mechanics and microscopic theoretical approaches, Soft Matter 10 (13) (2014) 2213–2225.
[34] D. Garcia-Gonzalez, M. Hossain, A microstructural-based approach to model magneto-viscoelastic materials at finite strains, Int. J. Solid Struct. 208 (2021) 119–1132.
[35] R. Zabihyan, J. Mergheim, A. Javili, P. Steinmann, Aspects of computational homogenization in magneto-mechanics: boundary conditions, RVE size and microstructure composition, Int. J. Solid Struct. 130 (2018) 105–121.
[36] P.P. Castañeda, E. Galipeau, Homogenization-based constitutive models for magnetorheological elastomers at finite strain, J. Mech. Phys. Solid. 59 (2) (2011) 194–215.
[37] R. Zabihyan, J. Mergheim, J. Pelteret, B. Brands, P. Steinmann, FE2 simulations of magnetorheological elastomers: influence of microscopic boundary conditions, microstructures and free space on the macroscopic responses of MREs, Int. J. Solid Struct. 193 (2020) 338–356.
[38] U.R. Poojary, K. Gangadharan, Material modeling of frequency, magnetic field and strain dependent response of magnetorheological elastomer, J. Mater. Sci. (2021) 1–15.
[39] B. Wang, L. Kari, A nonlinear constitutive model by spring, fractional derivative and modified bounding surface model to represent the amplitude, frequency and the magnetic dependency for Magneto-sensitive rubber, J. Sound Vib. 438 (2019) 344–352.
[40] G. Zhu, Y. Xiong, Z. Li, L. Xiao, M. Li, X.F. Bai, A nonlinear dynamic model of magnetorheological elastomers in magnetic fields based on fractional viscoelasticity, J. Intell. Mater. Syst. Struct. 32 (2) (2021) 228–239.
[41] B. Wang, L. Kari, One dimensional constitutive model of isotropic magneto-sensitive rubber under shear deformation with amplitude, frequency and magnetic dependency, IOP Conf. Ser. Mater. Sci. Eng. 855 (1) (2020), 012002.

[42] J. Lejon, B. Wang, L. Kari, A constitutive model of the dynamic shear modulus dependence on temperature, prestrain, dynamic strain amplitude and magnetic field for magneto-sensitive elastomer, Int. J. Solid Struct. 219 (2021) 106–119.
[43] A. Dorfmann, I. Brigadnov, Constitutive modelling of magneto-sensitive Cauchy-elastic solids, Comput. Mater. Sci. 29 (3) (2004) 270–282.
[44] A. Dorfmann, R. Ogden, Some problems in nonlinear magnetoelasticity, Z. Angew. Math. Phys. 56 (4) (2005) 718–745.
[45] P. Saxena, M. Hossain, P. Steinmann, A theory of finite deformation magneto-viscoelasticity, Int. J. Solid Struct. 50 (24) (2013) 3886–3897.
[46] K. Danas, S. Kankanala, N. Triantafyllidis, Experiments and modeling of iron-particle-filled magnetorheological elastomers, J. Mech. Phys. Solid. 60 (1) (2012) 120–138.
[47] R. Bustamante, Transversely isotropic nonlinear magneto-active elastomers, Acta Mech 210 (3) (2010) 183–214.
[48] M. Shariff, R. Bustamante, M. Hossain, P. Steinmann, A novel spectral formulation for transversely isotropic magneto-elasticity, Math Mech 22 (5) (2017) 1158–1176.
[49] B. Wang, L. Kari, A visco-elastic-plastic constitutive model of isotropic magneto-sensitive rubber with amplitude, frequency and magnetic dependency, Int. J. Plast. 132 (2020) 102756.
[50] B. Wang, L. Kari, Constitutive model of isotropic magneto-sensitive rubber with amplitude, frequency, magnetic and temperature dependence under a continuum mechanics basis, Polymers 13 (3) (2021) 472.
[51] K. Haldar, B. Kiefer, A. Menzel, Finite element simulation of rate-dependent magneto-active polymer response, Smart Mater. Struct. 25 (10) (2016) 104003.
[52] L. Wang, Y. Kim, C.F. Guo, X. Zhao, Hard-magnetic elastica, J. Mech. Phys. Solid. 142 (2020) 104045.
[53] K. Danas, N. Triantafyllidis, Instability of a magnetoelastic layer resting on a non-magnetic substrate, J. Mech. Phys. Solid. 69 (2014) 67–83.
[54] M. Rambausek, K. Danas, Bifurcation of magnetorheological film–substrate elastomers subjected to biaxial pre-compression and transverse magnetic fields, Int. J. Non Lin. Mech. 128 (2021) 103608.
[55] A. Alberdi-Muniain, N. Gil-Negrete, L. Kari, Influence of carbon black and plasticisers on dynamic properties of isotropic magnetosensitive natural rubber, Plast Rubber Compos 41 (7) (2012) 310–317.
[56] P. Blom, L. Kari, The frequency, amplitude and magnetic field dependent torsional stiffness of a magneto-sensitive rubber bushing, Int. J. Mech. Sci. 60 (1) (2012) 54–58.
[57] J. Lejon, L. Kari, Preload, frequency, vibrational amplitude and magnetic field strength dependence of magnetosensitive rubber, Plast Rubber Compos 38 (8) (2009) 321–326.
[58] P. Blom, L. Kari, Amplitude and frequency dependence of magneto-sensitive rubber in a wide frequency range, Polym. Test. 24 (5) (2005) 656–662.
[59] K.L. Pickering, S.R. Khimi, S. Ilanko, The effect of silane coupling agent on iron sand for use in magnetorheological elastomers Part 1: surface chemical modification and characterization, Composer Part A Appl Sci Manuf 68 (2015) 377–386.
[60] L. Bodelot, J.-P. Voropaieff, T. Pössinger, Experimental investigation of the coupled magneto-mechanical response in magnetorheological elastomers, Exp. Mech. 58 (2) (2018) 207–221.
[61] T. Pössinger, C. Bolzmacher, L. Bodelot, N. Triantafyllidis, Influence of interfacial adhesion on the mechanical response of magneto-rheological elastomers at high strain, Micro Syst. 20 (4–5) (2014) 803–814.
[62] T.H. Nam, I. Petríková, B. Marvalová, Experimental and numerical research of stress relaxation behavior of magnetorheological elastomer, Polym. Test. 93 (2021) 106886.
[63] T.H. Nam, I. Petríková, B. Marvalová, Experimental characterization and viscoelastic modeling of isotropic and anisotropic magnetorheological elastomers, Polym. Test. 81 (2020) 106272.
[64] T. Huu Nam, I. Petríková, B. Marvalová, Effects of loading rate, applied shear strain, and magnetic field on stress relaxation behavior of anisotropic magnetorheological elastomer, Mech. Adv. Mater. Struct. (2021) 1–16.
[65] W. Jiang, J. Yao, X. Gong, L. Chen, Enhancement in magnetorheological effect of magnetorheological elastomers by surface modification of iron particles, Chin. J. Chem. Phys. 21 (1) (2008) 87.
[66] L. Chen, X. Gong, W. Jiang, J. Yao, H. Deng, W. Li, Investigation on magnetorheological elastomers based on natural rubber, J. Mater. Sci. 42 (14) (2007) 5483–5489.
[67] J. Li, X. Gong, Z. Xu, W. Jiang, The effect of pre-structure process on magnetorheological elastomer performance, Int J Mater 99 (12) (2008) 1358–1364.
[68] X. Gong, G. Liao, S. Xuan, Full-field deformation of magnetorheological elastomer under uniform magnetic field, Appl. Phys. 100 (21) (2012) 211909.
[69] G. Liao, X. Gong, S. Xuan, Magnetic field-induced compressive property of magnetorheological elastomer under high strain rate, Ind. Eng. Chem. 52 (25) (2013) 8445–8453.
[70] A. Boczkowska, S.F. Awietjan, S. Pietrzko, K.J. Kurzydłowski, Mechanical properties of magnetorheological elastomers under shear deformation, Compos. B Eng. 43 (2) (2012) 636–640.
[71] J. Zhang, H. Pang, Y. Wang, X. Gong, The magneto-mechanical properties of off-axis anisotropic magnetorheological elastomers, Compos. Sci. Technol 191 (2020) 108079.
[72] S. Abramchuk, E. Kramarenko, D. Grishin, G. Stepanov, L. Nikitin, G. Filipcsei, et al., Novel highly elastic magnetic materials for dampers and seals: part II. Material behavior in a magnetic field, Polym. Adv. Technol. 18 (7) (2007) 513–518.
[73] S. Abramchuk, E. Kramarenko, G. Stepanov, L. Nikitin, G. Filipcsei, A. Khokhlov, et al., Novel highly elastic magnetic materials for dampers and seals: Part I. Preparation and characterization of the elastic materials, Polym. Adv. Technol. 18 (11) (2007) 883–890.
[74] T. Tian, M. Nakano, Fabrication and characterisation of anisotropic magnetorheological elastomer with 45 iron particle alignment at various silicone oil concentrations, J. Intell. Mater. Syst. Struct. 29 (2) (2018) 151–159.
[75] Z. Varga, G. Filipcsei, M. Zrínyi, Magnetic field sensitive functional elastomers with tuneable elastic modulus, Polymer 47 (1) (2006) 227–233.
[76] L. Mullins, Softening of rubber by deformation, Rubber Chem. Technol. 42 (1) (1969) 339–362.
[77] K. Nishi, M.L. Kilfoil, C.F. Schmidt, F. MacKintosh, A symmetrical method to obtain shear moduli from microrheology, Soft Matter 14 (19) (2018) 3716–3723.
[78] J. Lejon, L. Kari, Measurements on the temperature, dynamic strain amplitude and magnetic field strength dependence of the dynamic shear modulus of magnetosensitive elastomers in a wide frequency range, J. Vib. Acoust. 135 (6) (2013).
[79] A.K. Bastola, M. Hossain, A review on magneto-mechanical characterizations of magnetorheological elastomers, Compos. B Eng. (2020) 108348.
[80] M. Cheng, W. Chen, Experimental investigation of the stress–stretch behavior of EPDM rubber with loading rate effects, Int. J. Solid Struct. 40 (18) (2003) 4749–4768.
[81] P. Forquin, M. Nasraoui, L. Siad, A. Rusinek (Eds.), An Experimental Method of Measuring the Quasi-Static and Dynamic Confined Behaviour of PMMA. EPJ Web Conf, EDP Sciences, 2010.
[82] A. Kara, A. Tasdemirci, M. Guden, Modeling quasi-static and high strain rate deformation and failure behavior of a (±45) symmetric e-glass/polyester composite under compressive loading, Mater. Des. 49 (2013) 566–574.
[83] A.D. Drozdov, A. Dorfmann, The payne effect for particle-reinforced elastomers, Polym. Eng. Sci. 42 (3) (2002) 591–604.
[84] L. Kari, On the dynamic stiffness of preloaded vibration isolators in the audible frequency range: modeling and experiments, J. Acoust. Soc. Am. 113 (4) (2003) 1909–1921.
[85] C. Norwood, J. Dickens, The effect of vibration isolator properties and structural stiffness on isolator performance, J. Vib. Control 4 (3) (1998) 253–275.